SCIENTIFIC REPORTS

OPEN

Single laser pulse generates dual photoacoustic signals for differential contrast photoacoustic imaging

Fei Gao[1,2], Xiaohua Feng[1], Ruochong Zhang[1], Siyu Liu[1], Ran Ding[1], Rahul Kishor[1] & Yuanjin Zheng[1]

Photoacoustic sensing and imaging techniques have been studied widely to explore optical absorption contrast based on nanosecond laser illumination. In this paper, we report a long laser pulse induced dual photoacoustic (LDPA) nonlinear effect, which originates from unsatisfied stress and thermal confinements. Being different from conventional short laser pulse illumination, the proposed method utilizes a long square-profile laser pulse to induce dual photoacoustic signals. Without satisfying the stress confinement, the dual photoacoustic signals are generated following the positive and negative edges of the long laser pulse. More interestingly, the first expansion-induced photoacoustic signal exhibits positive waveform due to the initial sharp rising of temperature. On the contrary, the second contraction-induced photoacoustic signal exhibits exactly negative waveform due to the falling of temperature, as well as pulse-width-dependent signal amplitude. An analytical model is derived to describe the generation of the dual photoacoustic pulses, incorporating Gruneisen saturation and thermal diffusion effect, which is experimentally proved. Lastly, an alternate of LDPA technique using quasi-CW laser excitation is also introduced and demonstrated for both super-contrast *in vitro* and *in vivo* imaging. Compared with existing nonlinear PA techniques, the proposed LDPA nonlinear effect could enable a much broader range of potential applications.

Photoacoustic (PA) technique has been attracting wide range of research interest in recent decade for biomedical imaging[1–13]. Due to the hybrid merit of optical absorption and ultrasound detection, PA technique has successfully overcome the long-standing challenge of optical diffusion in deep scattering medium, achieving sensitive optical absorption contrast and scalable spatial resolution[14–20]. To induce strong enough PA signal, high-power nanosecond pulsed laser is usually utilized as the light source[21–24]. With ultrashort laser pulse (e.g. 1~10 ns), both thermal and stress confinements are satisfied to obtain optimized conversion efficiency from light absorption to ultrasound emission. When one pulse is illuminated on the target, one PA signal could be induced through transient absorption, heating and thermal expansion. However, there is no literature reporting using one laser pulse to generate two nonlinearly correlated PA signals. We report a PA technique based on long laser pulse induced dual PA (LDPA) nonlinear effect, which, for the first time, enables two nonlinearly correlated PA signals' generation from one laser illumination. To induce two PA signals from one laser pulse, two sharp laser intensity transitions are required. Therefore we employ square-profile laser illumination, rather than Gaussian-profile of conventionally used laser source. Due to the sharp rising and falling edges of the square laser pulse, two PA signals originating from thermal expansion and contraction respectively, are expected to be generated. In addition, the laser pulse width should be long enough (larger than stress confinement time), so that the expansion-induced and contraction-induced PA signals could be separated in time domain. It is also expected that the two PA signals should show phase-inverted (180 degree difference) waveforms due to the separate expansion and contraction effects. More interestingly, the two PA signals should exhibit different signal strengths that may vary with different laser pulse width, which are caused by the concurrent heat accumulation and diffusion during the long laser

[1]School of Electrical and Electronic Engineering, Nanyang Technological University, Singapore, Singapore. [2]School of Information Science and Technology, ShanghaiTech University, Shanghai, China. Fei Gao and Xiaohua Feng contributed equally to this work. Correspondence and requests for materials should be addressed to Y.Z. (email: yjzheng@ntu.edu.sg)
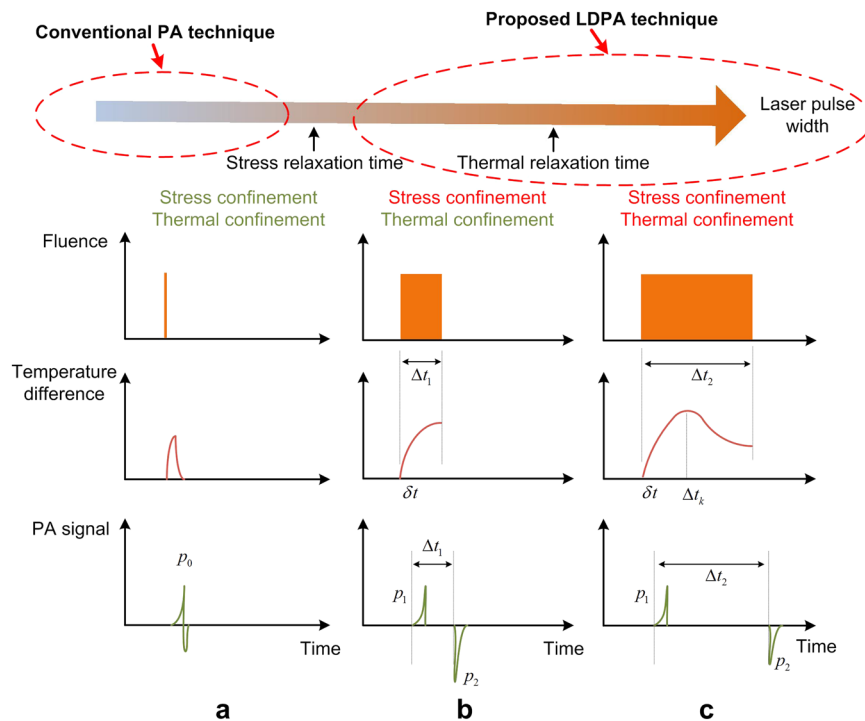
Figure 1. The fluence pattern, temperature change and PA signal waveform of (**a**) conventional short laser pulse induced PA effect with both stress and thermal confinements satisfied; (**b**) long laser pulse induced dual PA nonlinear effect with only thermal confinement satisfied, and (**c**) even longer laser pulse without thermal confinement.

pulse illumination (thermal confinement is not strictly met). Being clearly distinct from other reported thermal nonlinear PA technique that only happens when laser fluence exceeds a threshold value[25–27], the proposed LDPA nonlinear effect could be observed with low-power laser diode and applied in much broader range of applications. The nonlinearity of the LDPA effect could immediately enables several interesting applications, such as PA imaging with improved axial resolution[28], PA-guided optical focusing[29], and some more applications[30, 31]. Moreover, the pulse-width-dependent feature of the LDPA nonlinear effect could provide a characterization tool of different materials, and more importantly, it could also give design guideline for synthesizing advanced materials and nanoparticles to enhance the PA nonlinearity. In this paper, an analytical model is derived to describe the proposed LDPA nonlinear effect, and proof-of-concept experiments are performed to demonstrate its feasibility. The potential applications utilizing the LDPA effect are also discussed.

Results

Conventionally the short laser pulse with nanosecond pulse-width is used to induce transient temperature change in the optical absorber with both stress and thermal confinements, and a bipolar PA signal is generated following the thermoelastic expansion and contraction (Fig. 1a). To further increase the laser pulse-width to be larger than stress relaxation time ($\Delta t_1 > \tau_s = d/v$, d is the PA source diameter, v is the acoustic velocity), the single bipolar PA signal is gradually separated into two independent but correlated PA signals. The first pulse is expansion-induced positive PA signal p_1, the second pulse is contraction-induced negative PA signal p_2 with exactly inverted waveform (Fig. 1b). The first PA signal is generated immediately after the sharp temperature rise of the laser illumination, which is related with the light irradiation ϕ (W/cm^2) within short rising period δt. The analytical expression of p_1 is similar with the conventional short laser pulse induced PA:

$$p_1 = \Gamma_0 \eta_{th} \mu_a \phi \delta t, \tag{1}$$

where Γ_0 is the Gruneisen coefficient at the ambient temperature. η_{th} is the conversion efficiency from heat to pressure, and μ_a is the optical absorption coefficient.

On the other hand, the second PA signal p_2 could exhibit larger amplitude than the first one, which could be caused by more light energy deposition in the object, and higher Gruneisen coefficient (thermal expansion coefficient increased) due to the temperature rising of the object (Fig. 1b). However, when the laser pulse-width is further increased to larger than thermal relaxation time ($\Delta t_2 > \tau_{th} = d^2/\alpha$, α is the thermal diffusivity of the object), the amplitude of p_2 will be close to the amplitude of p_1, which is due to the significant thermal diffusion during the long laser illumination. Incorporating the Gruneisen increase, heat deposition and diffusion, the analytical expression of p_2 could be derived as below (Supplementary Note 1)[28, 29]:

$$p_2 = \left\{ \Gamma_0 + b\eta_{th}\mu_a\tau_{th}^2\phi\left[1 - \left(1 + \frac{\Delta t}{\tau_{th}} \right)e^{-\frac{\Delta t}{\tau_{th}}} \right] \right\}\eta_{th}\mu_a\phi\delta t + \Gamma_0\eta_{th}\mu_a \cdot \phi\Delta t \cdot e^{-\frac{\Delta t}{\tau_{th}}},$$

(2)

where b is the coefficient relating the absorbed thermal energy to the Gruneisen parameter change, and Δt is the laser pulse-width. Compared with Eq. (1) of the first conventional linear PA, the second PA signal p_2 shows nonlinearity governed by three terms in Eq. (2). The Gruneisen saturation term $b\eta_{th}\mu_a\tau_{th}^2\phi\left[1 - \left(1 + \frac{\Delta t}{\tau_{th}} \right)e^{-\frac{\Delta t}{\tau_{th}}} \right]$ describes the object's temperature rising and saturation due to heat accumulation during one laser pulse illumination. The light fluence $\phi\Delta t$ (J/cm^2) term is linearly increasing with laser pulse-width, and the thermal diffusion term $e^{-\frac{\Delta t}{\tau_{th}}}$ is exponentially decaying according to Newton's law of cooling due to temperature difference. The Gruneisen saturation term is derived by the time integration of heat deposition and diffusion (Supplementary Note 2). A quick observation of Eq. (2) shows that with increasing pulse width Δt, the first term with Gruneisen saturation in Eq. (2) increase. However, the second term in Eq. (2) may increase first due to the linearly increasing fluence, and then exponentially decrease due to the thermal diffusion. To analyze Eq. (2) quantitatively, we simplify the Eq. (2) by substituting some parameters with three constants: $A = \Gamma_0\eta_{th}\mu_a\phi\delta t = p_1$, $B = b\eta_{th}^2\mu_a^2\phi^2\delta t$, $C = \Gamma_0\eta_{th}\mu_a\phi$. Then Eq. (2) could be expressed as:

$$p_2 = p_1 + B\tau_{th}^2\left[1 - \left(1 + \frac{\Delta t}{\tau_{th}} \right)e^{-\frac{\Delta t}{\tau_{th}}} \right] + C\Delta te^{-\frac{\Delta t}{\tau_{th}}}$$

(3)

To obtain the optimum laser pulse width for maximizing the amplitude of p_2, the derivative of Eq. (3) is calculated (Supplementary Note 3) and expressed as below:

$$\frac{\partial p_2}{\partial \Delta t} = \left[C + \left(B - \frac{C}{\tau_{th}} \right)\Delta t \right]e^{-\frac{\Delta t}{\tau_{th}}}$$

(4)

To let $\partial p_2/\partial \Delta t = 0$ for maximum p_2 amplitude, we obtain the optimum laser pulse width:

$$\Delta t_0 = \frac{C}{\frac{C}{\tau_{th}} - B}$$

(5)

It indicates that the optimum laser pulse width Δt_0 doesn't always have a positive value. To be clear, the analysis is divided as below cases:

1) $C < B\tau_{th} \Rightarrow \Delta t_0 < 0$

For this case, there is no positive optimum laser pulse width. From Eq. (3) and smaller constant C than $B\tau_{th}$, the Gruneisen saturation term will dominate, and Eq. (3) could be simplified as:

$$p_2 = p_1 + B\tau_{th}^2\left[1 - \left(1 + \frac{\Delta t}{\tau_{th}} \right)e^{-\frac{\Delta t}{\tau_{th}}} \right]$$

(6)

It shows that with increasing laser pulse width, the amplitude of the second LDPA signal is expected to increase accordingly until saturation (Fig. 1b). This case is similar with the thermal nonlinear PA technique using two consequent short high-power laser pulses, where the second PA pulse is nonlinearly enhanced by the Gruneisen relaxation effect induced by the first pulse's heating[28, 29]. However, the proposed method could enable significant thermal nonlinearity by simply tuning the laser pulse width for sufficient heating accumulation using low power CW laser, and the temperature can easily rise sufficiently for nonlinear PA imaging, even reach tens of degrees increase for concurrent photothermal therapy. On the other hand, the two short consequent pulse method requires ultrahigh laser pulse energy and tight focusing to induce obvious temperature rise for the thermal nonlinear phenomenon.

Simulation under the condition $C < B\tau_{th}$ was conducted by sweeping the laser pulse width with different thermal relaxation time (20~100 μs) to calculate the nonlinear PA incremental amplitude ($p_2 - p_1$). The result shows that with increasing laser pulse width, the nonlinear PA amplitude increases gradually towards saturation (Fig. 2a), which is due to the heat accumulation and temperature rising. For larger value of thermal relaxation time, because of better thermal confinement property and heat accumulation, the nonlinear PA incremental amplitude increases more significantly than that with smaller thermal relaxation time. On the other hand, if the local temperature exceeds the boiling threshold of the medium (e.g. water) before saturation, bubble will be generated thereafter. It is worth noting that although longer laser pulse width is preferred to maximize the LDPA signal, the amplitude will reach saturation and there will be no significant increase when further increasing pulse width. As indicated by the dotted arrow line (Fig. 2a), A larger value of thermal relaxation time exhibits a longer increasing period, which requires longer laser pulse width to reach the saturation.

2) $C > B\tau_{th} \Rightarrow \Delta t_0 > 0$
For this case, there will be a positive optimum laser pulse width Δt_0 for maximum LDPA signal. When $C \gg B\tau_{th}$, the Eqs (3) and Eq. (5) could be simplified as $p_2 = C\Delta te^{-\frac{\Delta t}{\tau_{th}}}$ and $\Delta t_0 \approx \tau_{th}$, where Δt_0 is the
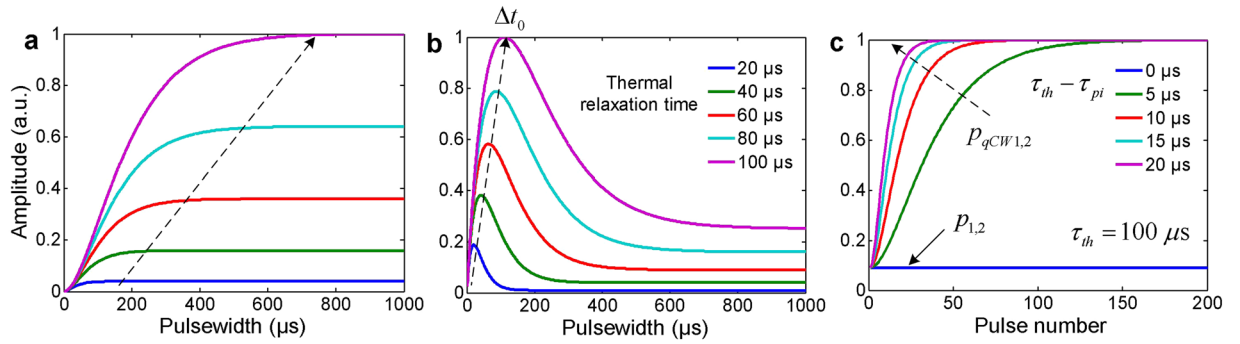
Figure 2. The simulation results of (**a,b**) The amplitude of the nonlinear PA incremental amplitude versus laser pulse width with different thermal relaxation time under case 1 and case 2. The dotted arrow line indicates the laser pulse width when the maximum LDPA amplitude is achieved. (**c**) The amplitude of the nonlinear PA amplitude versus laser pulse number with different pulse-pulse intervals (thus different $\tau_{th} - \tau_{pi}$) under case 3 with constant thermal relaxation time 100 μs.

turning point from amplitude increase to decrease of the LDPA signal (Fig. 1c), which could be used as the nonlinear characterization feature. The straightforward way to characterize this PA nonlinearity is to sweep the pulse width Δt and analyze the amplitude of p_2. As expected, simulation result shows that with increase laser pulse width, the amplitude experiences increasing and then decreasing accordingly (Fig. 2b). Moreover, with larger thermal relaxation time indicated by the dotted arrow line (Fig. 2b), the nonlinear PA incremental amplitude increases significantly due to better thermal confinement capability of the target. Meanwhile, the key pulse width Δt_0 also increases for maximum PA nonlinearity. In this case, Note that a proper selection of the laser pulse width is crucial to maximize the nonlinear PA signal. More importantly, the key pulse width Δt_0 is a unique parameter that characterizes the thermal nonlinearity of different materials, which could be further utilized for contrast-enhanced imaging.

3) Higher pulse repetition rate in quasi-CW mode

Except the heat accumulation and diffusion within one laser pulse, the long-term heat accumulation and base temperature rising could also be significant when the laser pulse repetition rate (N pulses per second with pulse-pulse interval $\tau_{pi} = 1/N$) is increased. Both p_1 and p_2 will be affected by another quasi-CW temperature rise and saturation term as a function of pulse number n. The PA signal at quasi-CW mode could be expressed as a superposition of previous one pulse induced linear and nonlinear PA signal $p_{1,2}$ and the quasi-CW temperature rise and saturation term:

$$p_{qCW1,2} = p_{1,2} + B\tau_{th}^2 \left\{ 1 - \left[1 + \frac{(n-1)(\tau_{th} - \tau_{pi})}{\tau_{th}} \right] e^{-\frac{(n-1)(\tau_{th}-\tau_{pi})}{\tau_{th}}} \right\}, \tau_{th} - \tau_{pi} > 0 \tag{7}$$

Note that $\tau_{th} - \tau_{pi} > 0$, so that within two consequent laser pulses, the accumulated heat by the first laser pulse doesn't totally dissipate before arrival of second laser pulse. When $\tau_{th} - \tau_{pi} = 0$ or $n = 1$, Eq. (7) goes back to $p_{qCW1,2} = p_{1,2}$ due to no heat accumulation between consecutive pulses or only single pulse. Eq. (7) shows that the absolute temperature change caused by the increased number of laser pulses in quasi-CW mode will nonlinearly enhance the signal amplitude of both p_1 and p_2 until saturation at a fixed laser pulse width. This indicates the potential to immediately enable the concurrent temperature detection and close-loop control during photothermal treatment[32, 33]. In addition, it also shows that even for the linear PA signal p_1 with increased laser repetition rate working in a quasi-CW way, p_{qCW1} could also exhibit nonlinearity. The simulation results with constant thermal relaxation time 100 μs and different pulse-pulse intervals (0~20 μs) show that when increasing number of laser pulses, the amplitude of $p_{qCW1,2}$ increases until saturation (Fig. 2c). As expected, when $\tau_{th} - \tau_{pi} = 0$, the amplitude keeps constant due to no heating accumulation within pulse-pulse intervals. Lastly, as indicated by the dotted arrow line with $\tau_{th} - \tau_{pi}$ increasing, less number of laser pulses is required for the nonlinear PA signal to reach the maximum amplitude.

The experimental setup is like a typical PA microscopy system (Fig. 3a and **Methods**). The first observation of the LDPA nonlinear effect is from a black rubber wire sample, which has strong optical absorption at the laser's wavelength. For comparison, the conventional single PA signal could be generated by short laser pulse width. With 1 μs laser pulse width (Fig. 3b), only one PA signal could be generated (Fig. 3d). On the other hand, a typical measured waveform of LDPA signal with 10 μs laser pulse width (Fig. 3c) is shown in Fig. 3e. As expected, the delay between the two PA signals generated from rising and falling edges of pulse laser illumination is also 10 μs. The waveforms of the two PA signals show high correlation and inverted amplitude, which is caused by the initial expansion (first PA signal) and contraction (second PA signal) from the same optical absorber. In addition, the peak-to-peak amplitude of the second nonlinear PA signal is larger than that of first linear PA signal, which results from the heating accumulation and temperature rising during the laser pulse.
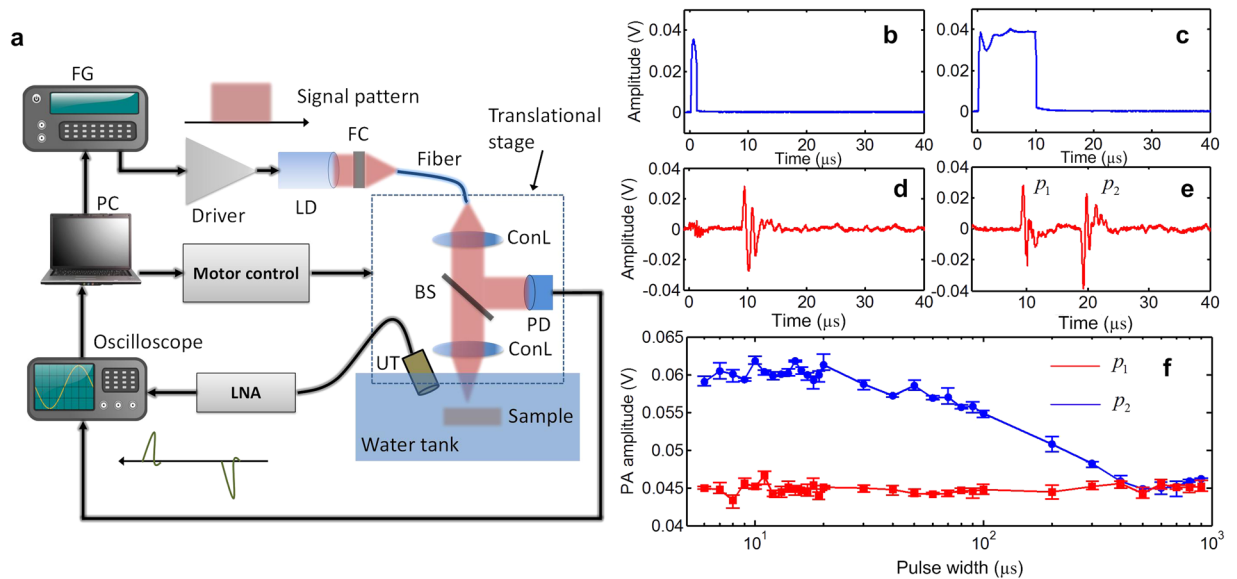
Figure 3. (**a**) The schematic of the experimental setup. FC: function generator; LD: laser diode; FC: fiber coupler; ConL: condenser lens; BS: beam splitter; PD: Photodiode UT: ultrasound transducer; LNA: low-noise amplifier. (**b,c**) The light illumination signal detected by the photodiode with pulse width of 1 μs and 10 μs. (**d,e**) The measured LDPA signals with 1 μs and 10 μs pulse width laser illumination. (**f**) Amplitudes of first PA signal (red line, square symbol) and second PA signal (blue line, circle symbol) by sweeping the pulse width of the laser source.

By sweeping the laser pulse width from 6 μs to 900 μs, the amplitudes of both first and second PA signals from the black rubber wire are recorded (Fig. 3f). As expected, the first PA signal's amplitude keeps almost constant when sweeping the laser pulse width, because the expansion-induced PA signal is generated by the rising edge of light illumination, and not influenced by the heat accumulation and diffusion during the long-pulse light illumination. However, the second PA signal, as well as the ratio between the two PA signals, experiences an increase (<10 μs), flat (10~20 μs) and decrease (20~500 μs) when sweeping the laser pulse width. The measurement result agrees well with the prediction in Fig. 2b when the thermal relaxation time of the medium is small ($C > B\tau_{th}$).

As predicted from Fig. 2a, when the thermal relaxation time of the medium is large enough ($C < B\tau_{th}$), the second nonlinear PA signal will keep rising when increasing the laser pulse width. To demonstrate this situation, we took black ink sealed in a plastic micro-tube as the testing sample to be immersed in water. Due to better heat isolation of the plastic layer compared with the previous black wire sample contacting water directly, the sealed black ink sample is expected to achieve much larger thermal relaxation time. By tuning the laser pulse width to be 100 μs, 500 μs and 1 ms, it is observed that the second nonlinear PA signal keeps increasing with larger laser pulse width as expected (Fig. 4a–c). Finally, when laser pulse width was further tuned to be 1.5 ms, the local temperature at the focal point reached the boiling point of water leading to bubble generation (Fig. 4d) and significantly enhanced PA signal generation. The comparison plot shows that the nonlinear ratio (p_2/p_1) of bubble-induced PA is around 450, much greater than the LDPA signals before bubble generation (Fig. 4e). The upper limit of the nonlinear ratio for the LDPA signals generated from water is around 3.5~4, which equivalently refers to the temperature rise from ambient temperature (~25 °C) to boiling point (~100 °C). To explore the temperature-dependent property of the LDPA effect, the repetition rate of the laser source (fixed pulse width: 10 μs, peak power: 1 W) was swept from 100 Hz to 1.9 kHz, which corresponds to average power sweeping from 1 mW to 19 mW. Figure 4f shows the amplitudes of the two PA signals versus average power sweeping. As expected, with increasing average power of the laser source, absolute temperature of the sample also increases. Then the elevated Gruneisen coefficient enhances both PA signals, which is predicted from Fig. 2c.

Although the heat accumulation and nonlinear PA enhancement could be obviously observed in the above measurement, the nonlinear PA signal's amplitude is relatively weak due to the low peak power of the CW laser source. To compensate the PA signal's amplitude as well as utilizing the merit of the proposed LDPA effect, here we further propose an alternative LDPA technique by using quasi-CW laser – a high-repetition-rate pulsed laser diode. As shown in Fig. 5a, the laser source excites *N* consecutive short laser pulses with high repetition rate, and the time interval between two adjacent laser pulses are short enough for quasi-continuous heat accumulation (the heat induced by previous laser pulse doesn't totally dissipate before the next laser pulse reaches). Therefore, the local temperature rising, as well as the thermal expansion coefficient of the object, could continuously accumulate during the N laser pulse sequence, leading to nonlinear enhanced PA signal amplitude.

By replacing the CW laser in the previous setup with a quasi-CW laser source (**Methods**), 500 consecutive laser pulses were illuminated on the black ink sample. As shown in Fig. 5b, the amplitudes of the 500 PA signals are increasing as expected, where the last nonlinear PA signal (Fig. 5d) exhibits significantly enhanced amplitude compared with the first linear PA signal (Fig. 5c). By quantitatively plotting the nonlinear increase percentage
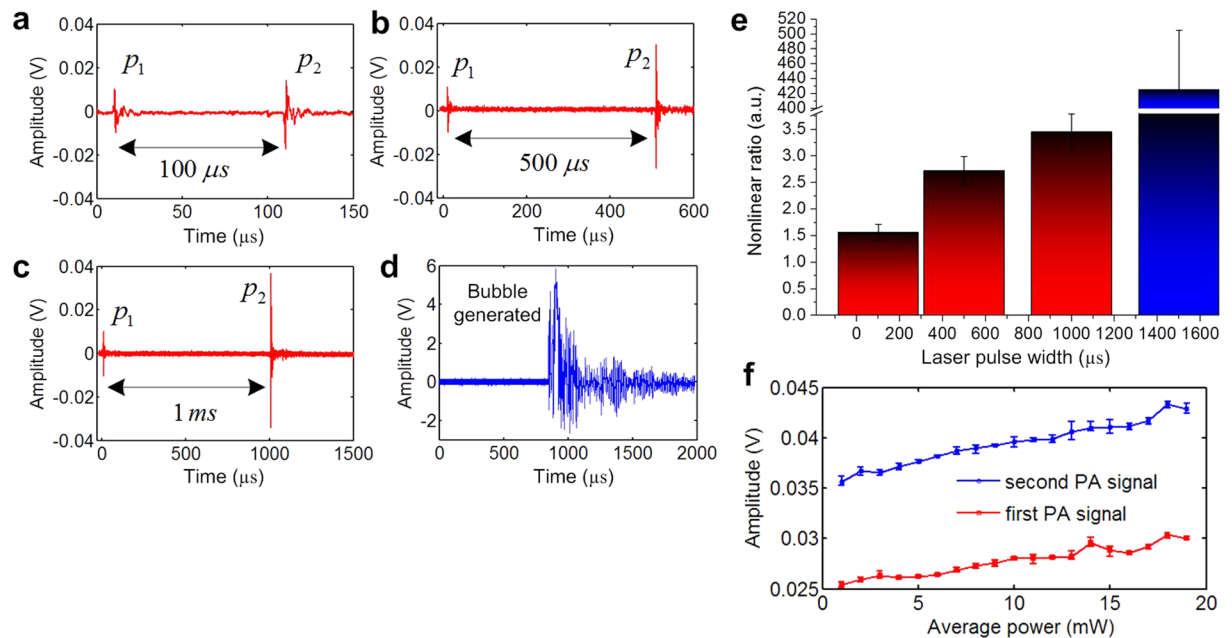
Figure 4. The measured LDPA signals from black ink with laser pulse width of (**a**) 100 μs, (**b**) 500 μs and (**c**) 1 ms. (**d**) Significant PA signal generation due to bubble generation and collapse with 1.5 ms laser pulse width. (**e**) The nonlinear ratio comparison with different laser pulse widths. (**f**) Amplitudes of first PA signal (red line, square symbol) and second PA signal (blue line, circle symbol) by sweeping the average power of the laser source.

versus number of pulses in Fig. 5e, we can see that ~80% enhancement is achieved by the LDPA technique with quasi-CW laser source. In comparison, only ~3% enhancement is achieved by using two consecutive laser pulses proposed in literature[28, 29]. It is expected that by further increasing the number of laser pulse, the nonlinear enhancement will increase and finally reach constant, which is caused by the balanced thermal accumulation and diffusion. Then, imaging results were acquired by raster-scanning over a curved black wire sample based on the LDPA technique by quasi-CW laser. The reconstructed images by the first linear PA signal, the last nonlinear PA signal, and the differential image are shown in Fig. 5f. As indicated in Fig. 5g, the image contrast of the nonlinear PA imaging shows a slight improvement (6.7:1) than the linear PA (5.9:1). However, the differential image contrast achieves a much greater improvement (14.8:1). The underlying reason is that by subtracting the linear PA image from nonlinear PA image, the pure nonlinear increase caused by the heat accumulation is extracted. At the same time, the linear absorption background is significantly suppressed by the subtraction[34–36]. Another set of experiments using a two lines phantom (Fig. 5h) was conducted by setting three different laser pulse number: 50, 75 and 100. Due to less pulse number, the nonlinear PA images (Fig. 5i) show slightly enhanced intensity than the linear PA image (Fig. 5h). However, the differential images again show more and more significantly enhanced image contrast with increasing pulse number.

Finally, *in vivo* imaging in rat based on the proposed LDPA nonlinear effect was performed to demonstrate the feasibility towards biomedical imaging applications. We developed the PA imaging system based on raster scanning and quasi-CW laser excitation (Fig. 6a and **Methods**) to acquire linear PA imaging, nonlinear PA imaging and differential imaging in single modality. Seven-week-old rat was used for the *in vivo* experiments with subcutaneous injection of a kind of NIR organic dye – IR-820 into the abdomen region (Supplementary Fig. S1 and **Methods**) considering the reason that organic materials could exhibit a quite low thermal conductivity and good thermal confinement property[37, 38]. As shown in Fig. 6b, due to the existence of blood spot at the surface of the abdomen skin, very strong PA signal was detected in the linear PA imaging result. However, the linear PA signal from the IR820 is overwhelmed by the strong PA signal from blood and not discernable. Then, the nonlinear PA image was acquired by reconstructing the last nonlinear PA signal of the pulse sequence. It is observed that the nonlinear PA signal from IR820 increases significantly due to its better thermal confinement and heat accumulation under the skin. On the other hand, the nonlinear PA signal from the skin blood spot is still very strong, but has subtle increase over their linear PA signals due to its much less thermal confinement and heat accumulation capability at the skin surface. By applying differential imaging, the image contrast of the IR820 over the blood background is further improved by suppressing the PA signal from blood with weak nonlinearity (Fig. 6c). The quantitative comparison shows that the image contrast is improved from 0.49 (linear PA imaging) to 1.7 (nonlinear PA imaging) and 12.3 (differential imaging) (Fig. 6d). Lastly, both linear and nonlinear PA imaging have also been performed on the rat's ear to demonstrate the improved image contrast (Fig. 6e,f). Future experiments could be conducted by injecting the dyes to the circulation, which is also expected be detected when they are aggregating at some spot, such as tumor or lymph node. Even when the dye is flowing inside the blood vessel, the detection may be also feasible, and we will explore further towards a LDPA flowmetry implementation.
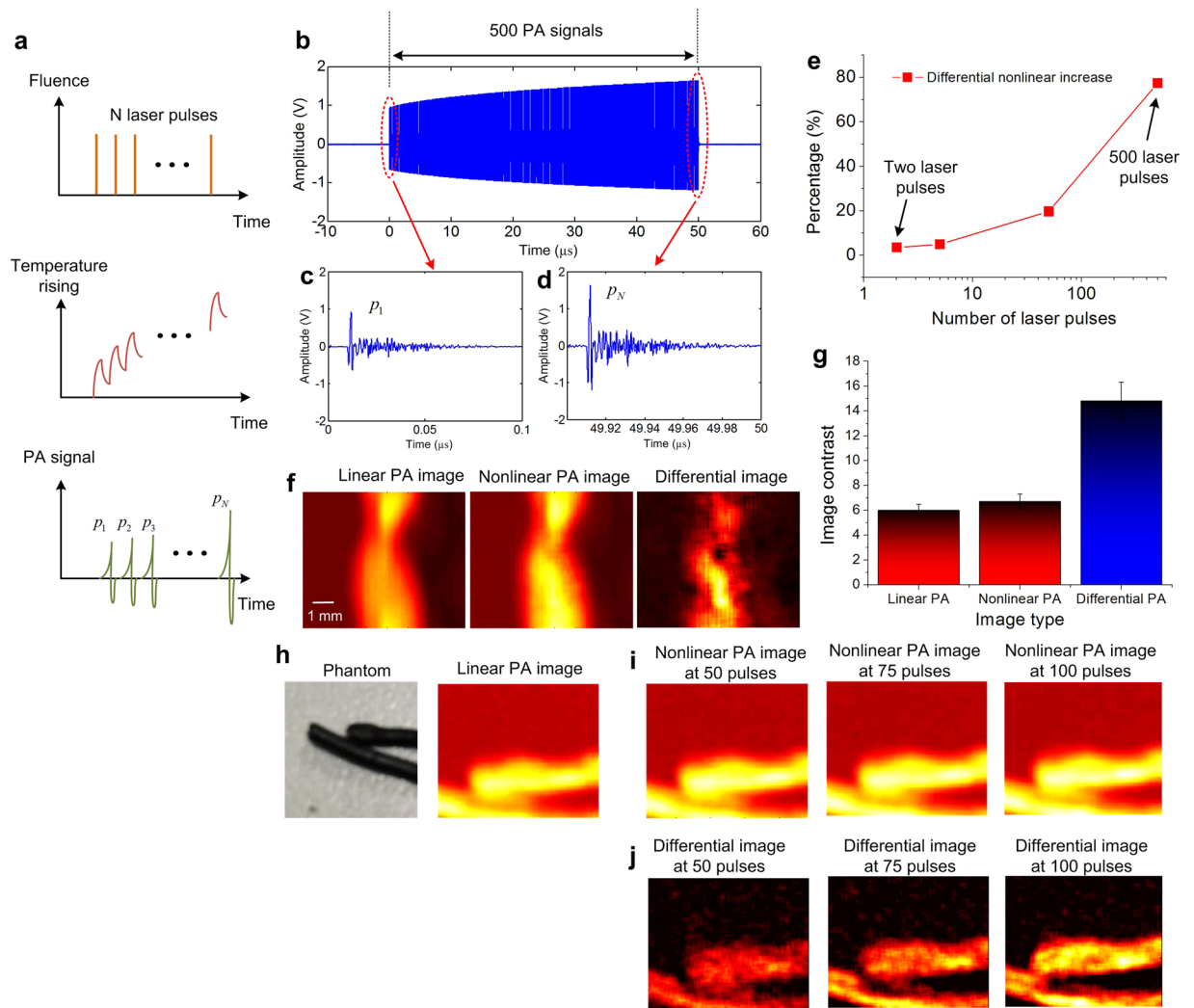
Figure 5. (**a**) The fluence pattern, temperature rising and PA signal diagram of the proposed LDPA technique by quasi-CW laser source. (**b**) A typical 500 PA signals, (**c**) the first linear PA signal, and (**d**) the last nonlinear PA signal. (**e**) The percentage of nonlinear increase versus the number of consecutive laser pulses. (**f**) The linear PA imaging, nonlinear PA imaging and differential imaging of a curved black wire, (**g**) and their quantitative comparison of imaging contrast. (**h**) The photograph of another two black wire phantom and its linear PA imaging. (**i**) The nonlinear PA imaging and (**j**) Differential imaging results at three different pulse numbers: 50, 75, 100.

Discussion

The first concern about the proposed long pulse PA method is safety issue. According to the ANSI limit (Z136.1–2000), the maximum permissible exposure (MPE) for 808 nm laser source is calculated as ~32 mJ/cm². For the long pulse laser excitation in this manuscript, a laser diode with 1 W peak power is used. When the laser pulse of 100 μs is selected, the laser energy per pulse is 0.1 mJ. The focal area is about 0.01 cm², so the laser fluence is 0.1 mJ/0.01 cm² = 10 mJ/cm², which is below the MPE. Fortunately, the experimental results have shown that long laser pulse with <100 μs pulse width is sufficient to induce obvious nonlinear PA signals. Except ANSI limit, another safety issue to be concerned is local temperature rising. According to the temperature sensitivity of PA signal (~5% per degree), a transient temperature rising of only 5 degree will render a PA signal enhancement of around 30%, which is also obvious enough for sensitive PA detection. The bubble generation by long laser pulse is not supposed to be used in real *in vivo* applications due to its destructive nature. Regarding the quasi-CW method, the fluence at the skin is calculated as 0.2 mJ/0.01 cm² = 20 mJ/cm², which is also below the MPE for 808 nm laser source. Considering the weak focusing and light scattering in the tissue, the fluence at the target is estimated to be smaller than that at the skin. To clarify this issue more clearly, at each scanning point, we need to consider ANSI standard for both pulse laser case (32 mJ/cm²) mentioned above, and CW/quasi-CW laser case (200 mW/cm²). To guarantee safety, both requirements need to be satisfied concurrently. For CW/quasi-CW laser case, at each scanning point, one long laser pulse of 100 μs pulse width carries 0.1 mJ laser energy, so within e.g. 100 seconds (actually only 1 pulse during the whole imaging process for each scanning point), the average power is only 0.1 mJ/100 s/0.01 cm² = 0.1 mW/cm². On the other hand for multi-pulse
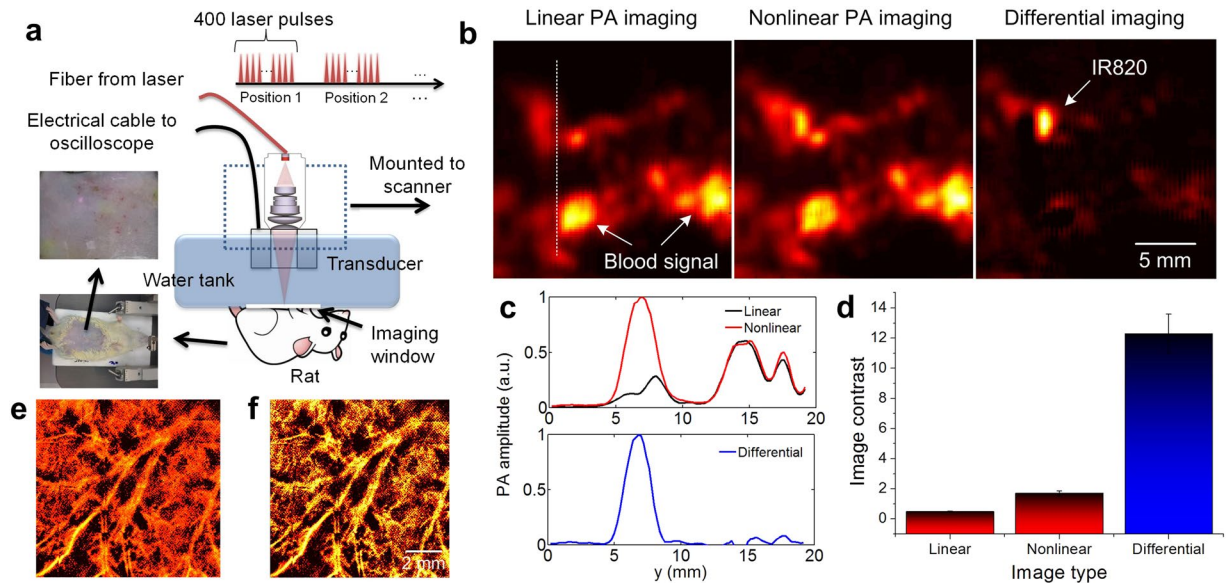
Figure 6. (**a**) *In vivo* experimental setup based on the LDPA technique by quasi-CW laser excitation. (**b**) The reconstructed linear PA, nonlinear PA and differential imaging results of a rat with subcutaneous injection of IR820 in the abdomen. Strong PA signals from high-absorptive blood background are shown in the linear and nonlinear PA images. By subtracting, the signal from the IR820 pops up with linear background suppression. (**c**) Normalized signal intensity of the linear, nonlinear and differential images along the white dashed line in b. (**d**) The image contrast comparison of the three images in b. (**e**) The linear PA imaging and (**f**) nonlinear PA imaging results of the ear vascular.

method, a pulse train of 500 laser pulses with 0.2 mJ for each pulse carries a total of $0.2 \times 500 = 100$ mJ energy, the average power is only 100 mJ$/100$ s$/0.01$ cm$^2 = 100$ mW/cm^2. They satisfy both ANSI standards. Furthermore, we acknowledge that there is always a tradeoff between performance and illumination power for the proposed methods. For example, to enhance PA signal's SNR, it may require multiple data acquisitions and averaging at each scanning point, posing higher laser fluence on the tissues. In addition, to scaling the focal spot to several micron meters for high-resolution imaging, the laser fluence also needs to reduce accordingly to satisfy the ANSI standard. Therefore, we need to carefully select proper laser parameters, including the laser pulse width, pulse train number, laser repetition rate, and data averaging number, to guarantee the safety of the biological tissue for further *in vivo* studies.

Due to the usage of low-peak-power laser source in this study, the PA signal amplitude is much weaker than the conventional PA imaging using high-peak-power laser source. Therefore, sensitivity, not resolution, is the key factor when choosing the frequency of ultrasound transducer for this study. So lower frequency is more preferred due to much smaller acoustic attenuation in low frequency range. Furthermore, considering the focal spot size (~1 mm^2), 1 MHz is an optimum choice covering the spectrum of PA signal that maximizes the detection sensitivity. Determined by the transducer's frequency and light focal spot size, the axial resolution is about 0.7 mm, and lateral resolution is about 1 mm for current setup. In the future work, higher frequency transducer will be utilized to achieve higher image resolution for more advanced applications. When spot size reduces to several microns for high-resolution imaging, the case needs to be re-considered carefully. Due to the much smaller spot size and heating volume, it is expected that the thermal relaxation time will be shortened significantly, which will impose more challenges on the thermal nonlinear PA generations. Specifically, the long pulse-width and pulse-interval should be reduced further to ensure the safety when getting better optical focusing, meanwhile guarantee sufficient heat accumulation and avoid significant thermal diffusion. Another challenge regarding the high-resolution microscopy is sensitivity, because we need to reduce the laser intensity within safety limit, as well as detecting high-frequency PA signal with severe acoustic attenuation. To address this challenge, we could increase the gain of low-noise amplifier and apply multiple data averaging, but meanwhile, decrease the pulse width, pulse number, and laser repetition rate to guarantee the laser safety. Regarding the imaging depth of the *in vivo* imaging results, it is about 1~2 mm below skin, which corresponds to the subcutaneous injection location of the nanoparticles. Further penetration depth could be expected due to the NIR light source. Regarding the imaging speed, the laser repetition rate is 10 kHz, and forming an image needs $100 \times 100 = 10000$ scanning points. Therefore, the time required is $10000/(10 \text{ kHz}/400) = 400$ seconds $= 6.6$ minutes. Compared to conventional single laser pulse induced PA imaging, the proposed quasi-CW LDPA method requires much more pulses at each scanning point. However, thanks to the high repetition rate of the laser source, the scanning speed is still satisfactory, and 6 min is still tolerable for many pre-clinical applications. The imaging speed could be further optimized by employing higher repetition rate laser, reducing pulse number at each point, and tomographic setup with ultrasound array probe.

	Dual-pulse nonlinear PA	Proposed LDPA by CW laser excitation	Proposed LDPA by Quasi-CW laser excitation
Physical mechanism			
Nonlinear origin	Impulse temperature rise then heat relaxation during laser interval	Continuous temperature rise and heat accumulation	Quasi-continuous temperature rise and heat accumulation
Physical conditions	Thermal and stress confinements satisfied for two PA generations	First PA signal: satisfied Second PA signal: unsatisfied	Thermal and stress confinements satisfied for all PA signals
PA generation mechanism	Two laser pulse induce two PA signals	One laser pulse induce two PA signals	N consecutive laser pulses induce N PA signals
System performance			
Heating efficiency	×Low (single short laser pulse heating)	√ High (continuous laser heating)	√ High (Quasi-continuous laser heating)
PA signal strength	√ High (high peak power pulsed laser)	×Low (low-power CW laser)	√ High (high peak power pulsed laser)
System cost	×Very high (two high-power laser systems required)	√ Very low (single CW laser diode)	√ Low (single high-rep-rate pulsed laser diode)
Applications	×Need tight focusing to improve the heating efficiency and nonlinearity (e.g. time-reversal optical focusing in scattering medium)	×Need strong absorber and focusing to improve the PA SNR (e.g. contrast-enhanced PA microscopy)	√ Generally applicable to most PA embodiments (e.g. PA tomography, microscopy, endoscopy, etc.)

Table 1. The comparison table between the proposed LDPA techniques with the existing dual-pulse nonlinear PA technique.

Regarding the applicability of the proposed method, generally speaking, all types of biological tissues can exhibit nonlinear PA enhancement by properly selecting pulse width/number. Due to the different compositions of different tissue types, they are expected to have different thermal relaxation properties, which form the basis of optimal enhancement for each specific tissue type. Moreover, even if some types of tissues are quite similar in terms of nonlinear PA enhancement, such as early-stage tumor and surrounding healthy tissue, it is still feasible to utilize engineered molecular probe (e.g. nanoparticles, or organic dyes) bounding to the tumor, achieving distinct LDPA nonlinear enhancement. The most significant advantage of utilizing LDPA nonlinear method is that it does not require a large dose of nanoparticles to induce much stronger PA signals than surrounding tissues. Small dose of nanoparticles can also provide obvious LDPA nonlinearity, even though their linear PA signal may be even smaller than that of surrounding tissues.

To better illustrate the merits of the proposed LDPA technique by both CW and quasi-CW laser source, Table 1 is provided below to compare it with the recently proposed dual-pulse nonlinear PA technique[28, 29]:

It shows that the three techniques differ in terms of both physical mechanism and system performance. Especially regarding heating efficiency and system cost, the proposed LDPA technique by CW laser exhibits much more advantageous than the existing dual-pulse nonlinear PA method. To overcome the low peak power of the CW laser source, the alternative LDPA technique by quasi-CW laser bridges the merits of the other two and achieves simultaneous high heating efficiency, high PA signal strength and low system cost. We would like to clarify that although the proposed LDPA technique shows some advantages compared with the dual-pulse approach in some aspects in this table, the dual-pulse approach is still showing strength in higher PA generation efficiency and better for short thermal relaxation time case. Therefore, appropriate selection among these techniques is highly suggested for various kinds of applications. Regarding the most potential application of the proposed LDPA technique, one of them could be contrast-enhanced PA imaging for early-stage tumor detection with intrinsic nonlinear PA contrast or exogenous nanoparticles. Validated by the preliminary *ex vivo* and

in vivo experiments above, further development of the proposed method is expected to be feasible. Moreover, more applications are still pending to be explored in our future work, e.g. the quantitative PA imaging providing function information.

In conclusion, we report the LDPA nonlinear effect with one pulse illumination by modulated CW laser and two PA signals detection. Then we extend it to an alternative LDPA technique by quasi-CW laser source for stronger PA signal strength. An analytical model is derived to model the LDPA effect. Then both *in vitro* and *in vivo* sensing and imaging have been performed to demonstrate the feasibility of the technique towards biomedical imaging applications. The proposed LDPA technique enables several interesting applications based on low-power low-cost laser diode. Nevertheless, the potential challenges and limitations of the proposed method cannot be neglected, e.g. very short thermal relation time and safety limitations in microscopic setup, and low sensitivity in deep tissue tomography. With today's technology, the method is not practical for real clinical applications, but possibly future technologies (e.g. much more sensitive detectors) might make this method feasible. Regarding the quantitative measure of e.g. oxygen saturation for functional imaging, the proposed LDPA method also meets challenge but still has potential to solve this problem according to some previous literature e.g.[39]. More studies are required to validate the proposed methods under different conditions, and for different applications in our future work. We would also wish to inspire other researchers in photoacoustic community to extend the capability of this method.

Methods

In vitro PA measurement based on LDPA effect by CW laser excitation.

As shown in Fig. 3a, the input square-wave pulse with tunable pulse width was generated by a function generator (33250A, Agilent), which was connected to a custom-designed current driver (maximum current: 5A). The output of the driver was then fed to a laser diode (L808P1000MM, Thorlabs, wavelength: 808 nm, power: 1W) with fiber coupling. The output light from the fiber (MHP550L02, Thorlabs) was then collimated and weakly focused by condenser lens (LB1471, Thorlabs) on the sample with spot size of ~500 μm. Meanwhile, a beam splitter (BSF10-B, Thorlabs) and photodiode (DET10A, Thorlabs) were utilized to monitor the laser intensity variation. An ultrasound transducer (V303-SU, Olympus) with 1 MHz central frequency was placed close to the sample. Both of the transducer and sample were immersed in water for optimum optical and acoustic coupling. The dual PA signals were firstly amplified by a low-noise amplifier (5662, Olympus), then recorded by an oscilloscope (WaveRunner 640Zi, LeCroy) with 100 MSPS sampling rate.

In vitro/vivo PA imaging based on LDPA effect by quasi-CW laser excitation.

The *in vivo* imaging setup (Fig. 6a) was updated based on the previous *in vitro* setup. Firstly, the CW laser source was replaced by a high-repetition-rate pulsed laser diode (Quantel Laser Diode Illuminator, wavelength: 808 nm, pulse width: 100 ns; rep. rate: 10 kHz; pulse interval: 100 μs; maximum pulse energy: 1 mJ (~0.2 mJ at the fiber output)) to output the consecutive laser pulse sequence working in a quasi-CW mode. Secondly, the imaging head was modified by integrating an objective lens (RMS4X, Thorlabs) and a custom-designed ultrasound transducer (I1C10NF, Doppler Inc.) with a hole inside in a confocal way to maximize the sensitivity. Lastly, the water tank was modified to accommodate the needs for *in vivo* imaging. A hole was cut at the bottom of the water tank, and then sealed by a thin transparent polyethylene membrane, which was directly placed on top of the skin of the rat's abdomen. To form an image, the imaging head was mounted to a 2D mechanical scanner for raster scanning over the sample. The step size is 200 μm over an imaging area of 2 cm, and the focal spot size is adjusted to about 1 mm² for deeper light delivery. A summary of the imaging system includes: PA signal SNR (>20 dB), image contrast (~12:1) the imaging resolution (0.7 mm, 1 mm), imaging speed (~6 min per image), penetration depth (1~2 mm), laser fluence (~20 mJ/cm²) and pulse energy (0.2 mJ).

Animal preparation.

A ten-weeks-old rat was used for this animal imaging study. This study conforms to the Guide for the Care and Use of Laboratory Animals published by the National Institutes of Health, USA and protocol approved by the Institutional Animal Care and Use Committee (IACUC), Nanyang Technological University. Through the experiment, the animal was anesthetized with 2% vaporized isofluorane. Hair around the region of abdomen was removed after hair removal lotion treatment. Then the IR-820 (volume: 0.1 ml, concentration: 2 mg/ml) was injected into the rat by subcutaneous injection. After some time of diffusion, the injected dye forms a spot with 1 mm × 2 mm size. After applying the ultrasound gel to optimize the acoustic coupling, the water tank was placed tightly on top of the rat's abdomen to ensure the good optic and acoustic coupling.

Imaging procedure.

1. Place the anesthetized rat on the animal holder and fix it, then place the water tank on top of the rat's abdomen. 2. Switch on the power of the imaging system and laser source, wait for 10 min for the warm-up. 3. Adjust the laser alignment and focusing, tune the position of the focal spot so that the PA signal observed from the oscilloscope is maximized. 4. Set the imaging area, scanning step, laser pulse width/number from the computer. 5. Start scanning process, at each scanning point, the computer sequentially triggers motor movement, laser firing, and data recording of oscilloscope. Meanwhile, raw data is transferred from oscilloscope to the computer by Ethernet port. 6. Image processing is done by the computer using MATLAB, peak-to-peak value is calculated for each PA signals at each scanning point to form the 2-D linear and nonlinear PA images. Image subtraction is performed to get the differential images.

IR-820 synthesis and characterization.

The IR-820 near-infrared dye and chloroauric acid (HAuCl4*3H2O) employed were commercially available and used without further purification unless specifically mentioned. IR-820 in aqueous solution exhibits peak absorption at 819 nm and still very strong absorption under the 808 nm wavelength of the laser used in the experiments (Fig. S1d). The biocompatibility of two near-infrared (NIR) dyes was quantitatively investigated by using 3-(4,5-dimethylthiazol-2-yl)-2,5-diphenyltetrazolium

bromide (MTT) assay based on the proliferations of HeLa cells. The cell viability could remain above 70% after the incubation with IR-820 dye at a high concentration of 5 mg mL−1 for 24 h (Fig. S1e), indicating its suitable biocompatibility.

Reference

1. Calasso, I. G., Craig, W. & Diebold, G. J. Photoacoustic point source. *Physical Review Letters* **86**, 3550–3553 (2001).
2. Emelianov, S. Y., Li, P. C. & O'donnell, M. Photoacoustics for molecular imaging and therapy. *Physics Today* **62**, 34–39 (2009).
3. Galanzha, E. I. *et al*. *In vivo* magnetic enrichment and multiplex photoacoustic detection of circulating tumour cells. *Nature Nanotechnology* **4**, 855–860 (2009).
4. Razansky, D. *et al*. Multispectral opto-acoustic tomography of deep-seated fluorescent proteins *in vivo*. *Nature Photonics* **3**, 412–417 (2009).
5. Ntziachristos, V. & Razansky, D. Molecular Imaging by Means of Multispectral Optoacoustic Tomography (MSOT). *Chemical Reviews* **110**, 2783–2794 (2010).
6. Beard, P. Biomedical photoacoustic imaging. *Interface Focus* **1**, 602–631 (2011).
7. Razansky, D., Buehler, A. & Ntziachristos, V. Volumetric real-time multispectral optoacoustic tomography of biomarkers. *Nature Protocols* **6**, 1121–1129 (2011).
8. Meng, J. & Song, L. Biomedical photoacoustics in China. *Photoacoustics* **1**, 43–48 (2013).
9. Dean-Ben, X.L. & Razansky, D. Adding fifth dimension to optoacoustic imaging: volumetric time-resolved spectrally enriched tomography. *Light-Science & Applications* **3** (2014).
10. Kim, C. & Razansky, D. Listening to Light and Seeing Through: Biomedical Photoacoustic Imaging. *Ieee Pulse* **6**, 3–4 (2015).
11. Manohar, S., van Apeldoorn, A. & Steenbergen, W. PHOTOACOUSTIC IMAGING Cells make themselves heard. *Nature Photonics* **9**, 216–218 (2015).
12. Gao, F., Feng, X. & Zheng, Y. Advanced photoacoustic and thermoacoustic sensing and imaging beyond pulsed absorption contrast. *Journal of Optics* **18**, 074006 (2016).
13. Strohm, E.M., Moore, M.J. & Kolios, M.C. Single Cell Photoacoustic Microscopy: A Review. *Ieee Journal Of Selected Topics In Quantum Electronics* **22** (2016).
14. Ntziachristos, V., Ripoll, J., Wang, L. H. V. & Weissleder, R. Looking and listening to light: the evolution of whole-body photonic imaging. *Nature Biotechnology* **23**, 313–320 (2005).
15. Tam, A. C. Applications of photoacoustic sensing techniques. *Reviews Of Modern Physics* **58**, 381–431 (1986).
16. Wang, L. V. Multiscale photoacoustic microscopy and computed tomography. *Nature Photonics* **3**, 503–509 (2009).
17. Wang, L. V. & Hu, S. Photoacoustic Tomography: *In Vivo* Imaging from Organelles to Organs. *Science* **335**, 1458–1462 (2012).
18. Wang, X. D. *et al*. Noninvasive laser-induced photoacoustic tomography for structural and functional *in vivo* imaging of the brain. *Nature Biotechnology* **21**, 803–806 (2003).
19. Xu, M. H. & Wang, L. H. V. Photoacoustic imaging in biomedicine. *Rev. Sci. Instrum* **77**, 041101 (2006).
20. Zhang, H. F., Maslov, K., Stoica, G. & Wang, L. V. Functional photoacoustic microscopy for high-resolution and noninvasive *in vivo* imaging. *Nature Biotechnology* **24**, 848–851 (2006).
21. Gao, F., Feng, X. & Zheng, Y. Photoacoustic phasoscopy super-contrast imaging. *Applied Physics Letters* **104** (2014).
22. Gao, F., Feng, X. & Zheng, Y. Photoacoustic elastic oscillation and characterization. *Optics express* **23**, 20617–20628 (2015).
23. Gao, F., Feng, X. H. & Zheng, Y. J. Coherent Photoacoustic-Ultrasound Correlation and Imaging. *IEEE Trans. Biomed. Eng.* **61**, 2507–2512 (2014).
24. Gao, F. *et al*. Fast photoacoustic-guided depth-resolved Raman spectroscopy: a feasibility study. *Optics letters* **40**, 3568–3571 (2015).
25. Prost, A., Poisson, F. & Bossy, E. Photoacoustic generation by a gold nanosphere: From linear to nonlinear thermoelastics in the long-pulse illumination regime. *Physical Review B* **92** (2015).
26. Simandoux, O., Prost, A., Gateau, J. & Bossy, E. Influence of nanoscale temperature rises on photoacoustic generation: Discrimination between optical absorbers based on thermal nonlinearity at high frequency. *Photoacoustics* **3**, 20–25 (2015).
27. Zharov, V. P. Ultrasharp nonlinear photothermal and photoacoustic resonances and holes beyond the spectral limit. *Nature Photonics* **5**, 110–116 (2011).
28. Wang, L., Zhang, C. & Wang, L.V. Grueneisen Relaxation Photoacoustic Microscopy. *Physical Review Letters* **113** (2014).
29. Lai, P., Wang, L., Tay, J. W. & Wang, L. V. Photoacoustically guided wavefront shaping for enhanced optical focusing in scattering media. *Nature Photonics* **9**, 126–132 (2015).
30. Shi, J.H., Wang, L.D., Noordam, C. & Wang, L.H.V. Bessel-beam Grueneisen relaxation photoacoustic microscopy with extended depth of field. *J. Biomed. Opt.* **20** (2015).
31. Wang, L. D., Li, G., Xia, J. & Wang, L. H. V. Ultrasonic-heating-encoded photoacoustic tomography with virtually augmented detection view. *Optica* **2**, 307–312 (2015).
32. Feng, X., Gao, F., Xu, C., Gaoming, L. & Zheng, Y. Self temperature regulation of photothermal therapy by laser-shared photoacoustic feedback. *Optics letters* **40**, 4492–4495 (2015).
33. Feng, X., Gao, F. & Zheng, Y. Photoacoustic-Based-Close-Loop Temperature Control for Nanoparticle Hyperthermia. *IEEE Trans. Biomed. Eng.* **62**, 1728–1737 (2015).
34. Yao, J. J. *et al*. Multiscale photoacoustic tomography using reversibly switchable bacterial phytochrome as a near-infrared photochromic probe. *Nature Methods* **13**, 67–73 (2016).
35. Feng, X., Gao, F. & Zheng, Y. Modulatable magnetically mediated thermoacoustic imaging with magnetic nanoparticles. *Applied Physics Letters* **106**, 153702 (2015).
36. Feng, X. H., Gao, F. & Zheng, Y. J. Thermally modulated photoacoustic imaging with super-paramagnetic iron oxide nanoparticles. *Optics letters* **39**, 3414–3417 (2014).
37. Qian, X., Gu, X.K. & Yang, R.G. Lattice thermal conductivity of organic-inorganic hybrid perovskite CH3NH3PbI3. *Applied Physics Letters* **108** (2016).
38. Pisoni, A. *et al*. Ultra-Low Thermal Conductivity in Organic–Inorganic Hybrid Perovskite CH3NH3PbI3. *The Journal of Physical Chemistry Letters* **5**, 2488–2492 (2014).
39. Danielli, A., Maslov, K., Favazza, C. P., Xia, J. & Wang, L. V. Nonlinear photoacoustic spectroscopy of hemoglobin. *Applied Physics Letters* **106**, 203701 (2015).

Author Contributions

Additional Information

Supplementary information accompanies this paper at doi:10.1038/s41598-017-00725-4

Competing Interests: The authors declare that they have no competing interests.

Publisher's note: Springer Nature remains neutral with regard to jurisdictional claims in published maps and institutional affiliations.